Int. J. Solids Structures, 1970, Vol. 6, pp. 519 to 538. Pergamon Press. Printed in Great Britain

LONGITUDINAL STRESS PULSE PROPAGATION IN NONUNIFORM ELASTIC AND VISCOELASTIC BARS

M. MAO and D. RADER

Department of Engineering and Applied Science, Yale University, New Haven, Connecticut

Abstract—Stress pulse propagation along homogeneous but nonuniform bars is investigated. The bars have two uniform end sections of different diameter joined by a finite transition region. When a pulse is incident on the transition it is distributed over an infinite network of paths leading to transmission and reflection. In the analysis the transition is approximated by a set of discrete steps in area. A finite set of paths which contribute significantly to the pulses of reflection and transmission are identified and included in the calculations for the two pulses. The basic analysis is suitable for elastic pulses of arbitrary shape and is reformulated in harmonic form for use in viscoelastic bars. Calculated and experimental results are found to be in good agreement.

1. INTRODUCTION

IN THIS paper, the propagation of uniaxial longitudinal stress pulses is investigated in bars having a region of continuously variable mechanical impedance. An analysis is presented wherein such regions are approximated by a set of discrete impedance steps.

The analysis is applicable whether the physical basis for variable impedance is inhomogeneity of material properties or nonuniformity of geometry. However, since it is more convenient to produce experimental specimens with prescribed geometry than with prescribed material properties, the problem is considered in the context of homogeneous but nonuniform bars.

Of specific interest is pulse propagation in elastic and viscoelastic bars having a single nonuniform region which serves as a transition between two uniform end sections. When a stress pulse impinges on the transition from one of the end sections there will be an infinite sequence of transmissions, reflections, reflections of reflections and so forth. Ultimately a net pulse of transmission and one of reflection can be observed in the end sections. In general these pulses will be distorted versions of the original pulse.

The earliest investigations of wave propagation along nonuniform or inhomogeneous bars were concerned with abrupt rather than gradual changes in impedance. Rayleigh [1] considered the propagation of extensional waves along an elastic wire having an abrupt change in impedance caused by joining two dissimilar segments; Kolsky and Lee [2] studied the transmission and reflection of a pulse incident on the junction between two viscoelastic bars of the same diameter; Ripperger and Abramson [3] considered extensional and flexural pulse propagation along an elastic bar in which an impedance jump was brought about by an abrupt change in cross section.

Other workers have investigated wave propagation in bars and plates having regions of continuously variable impedance. Thus, Donnell [4] discussed the transmission and reflection of waves in bars with gradual changes in diameter, and suggested that nonuniform regions be approximated by a set of discrete cylindrical elements. Reed [5] formulated a computer code to keep account of reflections and transmissions along paths through such

a set of discrete impedance steps. Lindholm and Doshi [6] obtained a solution for the transmission of an extensional pulse along a uniform bar in which the elastic modulus varied with position according to a simple power law.

In the present analysis it is possible to consider the transmission and reflection of a pulse of arbitrary shape passing through a region in which the variation in impedance is also arbitrary. This is done by tracing the paths of reflection and transmission through a sequence of discrete impedance elements approximating the region in a manner similar to that employed by Reed [5]. Requisite calculations are carried out at each impedance step of a subdivided transition region to determine the amplitudes of the reflected and transmitted portions of a pulse at that station. The sequence of calculations is ordered in such a way as to include only those selected paths through the transition which contribute significantly to the final transmitted and reflected pulses.

For the elastic problem, the incident pulse is approximated by a sequence of narrow rectangular pulses. A set of reflection and transmission coefficients is computed for an elemental rectangular pulse of unit amplitude incident on the transition region. These coefficients determine the transmission and reflection shapes for the elemental pulse and the results for an arbitrary incident pulse are obtained by superposition.

In the viscoelastic case, the coefficients of the elastic problem are incorporated in an analysis which is formulated in terms of sinusoidal wave trains. This is then applied to the Fourier spectrum of an arbitrary incident viscoelastic pulse.

The experimental specimens were given a simple geometry to facilitate machining. In each bar two uniform circular end sections were joined by a transition region in the form of a frustrum of a right circular cone. Pulses were produced by the impact of a steel ball at one end of a bar and were detected using paired semi-conductor strain gauges. The experimentally observed incident pulses are used as data for the calculations, the results of which are then compared with the experimental reflected and transmitted pulses.

2. ANALYSIS FOR ELASTIC BARS

The arrangement for the computational procedure is shown schematically in Figs. 1(a) and 1(b) for a conical transition in a bar with cylindrical end sections. In general, the transition will of course not be conical, but an arbitrary transition geometry can likewise be approximated by a set of uniform elements.

In each element it is assumed that the equation of motion given by the elementary theory of wave propagation along a uniform elastic bar can be used, i.e. the one dimensional wave equation. It is implicit in the elementary theory that the ratio of wavelength to bar radius is much greater than unity. For a pulse, this condition must be met by the wavelengths of the dominant harmonics in its Fourier spectrum. Thus for sufficiently long wavelengths lateral inertia can be ignored and the stress distribution is sensibly uniform through the cross section. The wave speed, c, is then a constant given by $c = (E/\rho)^{\frac{1}{2}}$ where E is Young's modulus and ρ the density.

In Fig. 1(a) the transition of length L is divided into any number of desired increments, each of length Δx. In the figure, there are 5 sections (6 junctions) for illustrative purposes. The junctions between elements are numbered consecutively in the direction of propagation of the incident pulse [Fig. 1(b)]. The elements are numbered in the same way, but the first element is taken to be the uniform section on the incidence side of the transition. Thus, junction j occurs between elements j and $j + 1$.

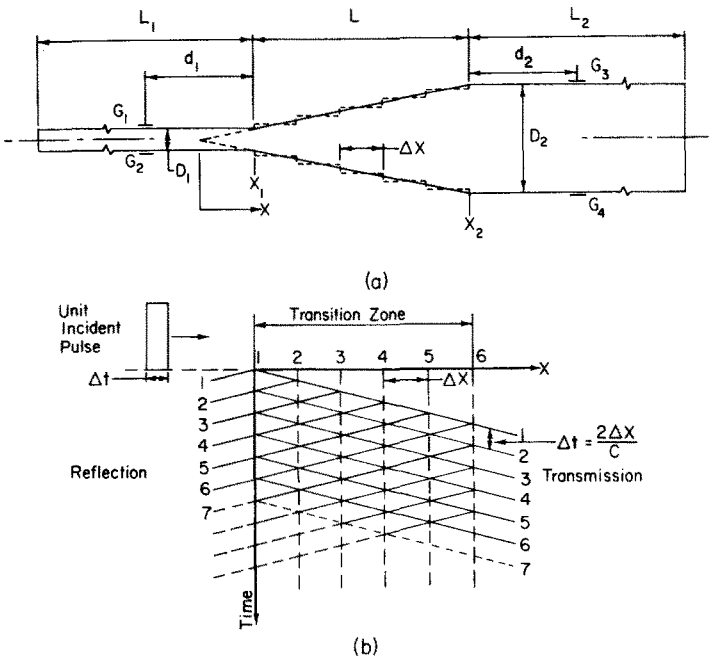

FIG. 1. (a) Bar geometry. (b) Path network in position–time plane.

At each junction the equations relating σ_i, σ_r and σ_t, the incident, reflected and transmitted stress amplitudes respectively, can be deduced starting from the well known solution to the wave equation (e.g. [1, 3, 7]). As a result of internal reflections incidence can occur from either side of a junction. Thus, if A_j and A_{j+1} are the cross sectional areas of adjacent elements, the sets of equations for reflection and transmission amplitudes at the jth junction are

$$\sigma_r = q_j\sigma_i, \qquad \sigma_t = p_j\sigma_i. \tag{1}$$

and

$$\sigma_r = \bar{q}_j\sigma_i, \qquad \sigma_t = \bar{p}_j\sigma_i \tag{2}$$

where

$$q_j = \frac{A_{j+1} - A_j}{A_{j+1} + A_j}, \qquad p_j = \frac{2A_j}{A_{j+1} + A_j} \tag{3}$$

and

$$\bar{q}_j = \frac{A_j - A_{j+1}}{A_{j+1} + A_j} = -q_j, \qquad \bar{p}_j = \frac{2A_{j+1}}{A_{j+1} + A_j}. \tag{4}$$

The unbarred quantities are appropriate when local incidence is in the direction of increasing j, and the barred quantities are appropriate when local incidence is in the opposite direction. In the more general case where material properties also vary, A_j and A_{j+1} are replaced by $\rho_j c_j A_j$ and $\rho_{j+1}c_{j+1}A_{j+1}$ respectively in (3) and (4). The cross sectional area

of each element is based on the mean value of the diameter of the transition region over the length Δx occupied by the element. In deriving (1) and (2) it is assumed that the angle of incidence is ninety degrees at each junction. This limits the local slope of the transition region to a reasonably small range of angles.

Consider now a rectangular stress pulse of unit amplitude [Fig. 1(b)] incident on the small end of the transition. It is convenient to choose the time duration of the pulse equal to twice the time of passage across a single element, i.e. $\Delta t = 2\Delta x/c$.

It is clear that the paths which lead to transmission and reflection [Fig. 1(b)] include only even and odd numbers of internal reflections respectively. From the definitions of q_j, p_j in (3) and $\bar{q}_j$, $\bar{p}_j$ in (4) one has in general

$$|q_j|, |\bar{q}_j| \ll 1 \text{ and } |p_j|, |\bar{p}_j| \simeq 1.$$

Thus the magnitude of a path contribution depends primarily upon the number of included reflections and it is useful to introduce the terminology of "path order". For transmission a first order or "primary" path includes two reflections, a second order or "secondary" path includes four reflections, and so forth. Similarly, for reflection, a primary path includes one internal reflection, a secondary path includes three internal reflections, and so forth. In the case of transmission there is also a special direct path which undergoes no reflections in passing through the transition region. This path leaves the transition on trajectory 1. The contribution of individual paths of successive orders evidently diminishes approximately by the factor q^2 for both reflection and transmission trajectories provided that $|q|$ is approximately constant along the transition length.

In general there will be a combination of primary, secondary and higher order path contributions leaving the transition region on the various exit trajectories of reflection and transmission. Thus it is convenient to categorize paths in groups according to their exit trajectories. The total amplitude of a group exiting from the transition on trajectory m, say, will be designated as α_m for the transmission trajectories and β_m for the reflection trajectories.

The coefficients can be written as the sum of contributions of a hierarchy of paths of several orders. Thus, in general,

$$\alpha_m = \alpha'_m + \alpha''_m + \alpha'''_m + \ldots \tag{5}$$

and

$$\beta_m = \beta'_m + \beta''_m + \beta'''_m + \ldots \tag{6}$$

where the number of primes on each term indicates the order of all paths included in that term. Except for the particular case when $m = 1$, the last term in (5) and (6) will include a single path of order $m - 1$. Thus one is able in principle to include all possible path contributions in a given group. In many cases of interest however, it is possible to neglect all but the lowest order contributions without introducing significant error.

This can be illustrated by considering the reflection trajectories for a transition region subdivided into k elements. It will be useful to first introduce the concept of "time zones", which are defined naturally by the round trip passage time of a wave over the length of

the transition. If there are k impedance elements, the first time zone ends at trajectory $m = k + 1$, the second at $m = 2k + 1$, the third at $m = 3k + 1$, and so forth. In each successive zone the lowest order path included in the previous zone is deleted. In Fig. 1b ($k = 5$) the first 6 trajectories fall within the first time zone and are shown as solid lines. The second time zone begins with trajectory 7 which is shown as a dashed line. Thus, there are no primary paths of reflection or transmission beyond trajectory 6.

For the reflection trajectories (in a transition of k elements) it will be noted that there is only a single primary path on each of the trajectories in the first time zone. There are no secondary paths in groups 1 and 2 but there is one included in group 3, three in group 4, six in group 5 and so on. Thus in the first time zone the number of secondary paths, η''_m, included in the mth reflection group is

$$\eta''_m = 1 + 2 + 3 + \ldots + m - 2 = \frac{(m-2)(m-1)}{2}, \qquad m = 3, 4, 5, \ldots, k+1. \tag{7}$$

Beyond the first time zone the secondary paths decrease in number with only one remaining on trajectory $m = 2k + 1$.

A somewhat more complicated analysis gives the following expression for η'''_m, the number of third order reflection paths within the first time zone:

$$\eta'''_m = \frac{(m-3)(m-2)^2(m-1)}{12}, \qquad m = 4, 5, 6, 7, \ldots, k+1. \tag{8}$$

In a typical case considered in this paper the number of impedance elements is $k = 20$ and the approximate mean value of the local reflection coefficient is $|q| = 0{\cdot}03$. In the first time zone the contribution of third order reflection paths is small relative to those of second order, but is greatest at $m = 21$. Thus, using (7) and (8), one has $(\eta'''_{21}/\eta''_{21})\, q^2 \simeq 0{\cdot}05$, or about 5 per cent, and further, one has $(\eta'''_{21}/\eta'_{21})\, q^2 \simeq 0{\cdot}01$ or about 1 per cent. Thus, in this example, it is reasonable to restrict calculations for β_m to primary and secondary paths in the first time zone. These restrictions are likewise applicable to the transmission paths. Primary and higher order transmission paths contribute chiefly to the tail of the transmitted pulse which is dominated by contributions along trajectory 1.

Numerical calculations for α_m and β_m are simplified considerably, as in the foregoing example, when the number of significant path orders and time zones can be ascertained. In most of the examples given in this paper it is possible to restrict calculations to primary and secondary paths in the first time zone without significant error.

However, in order to obtain an estimate of the relative contribution of two successive path orders, it is necessary that $|q|$ be reasonably uniform over the length of the transition region. For a conical transition this requires that the ratio of the terminating areas not be too great. When this is the case it follows in turn that the calculations can be satisfactorily restricted to primary and secondary paths in the first time zone although the details of the calculation depend upon the choice of k. If, however, the ratio of terminating areas is of the order of 10 or greater, $|q|$ changes rapidly along the transition and one finds that $|q|$ is relatively large near the small end of a conical transition. In such cases it is difficult to obtain reasonable estimates of path contributions and moreover the numerical calculations cannot be restricted to primary and secondary paths within the first time zone.

The procedure for calculating α_m and β_m can be illustrated using the typical path network of Fig. 1b. Considering the reflected pulse first, the primary path coefficients in the first time zone are

$$\begin{aligned}
\beta'_1 &= q_1 \\
\beta'_2 &= p_1 q_2 \bar{p}_1 \\
\beta'_3 &= p_1 p_2 q_3 \bar{p}_2 \bar{p}_1 \\
\beta'_4 &= p_1 p_2 p_3 q_4 \bar{p}_3 \bar{p}_2 \bar{p}_1 \\
\beta'_5 &= p_1 p_2 p_3 p_4 q_5 \bar{p}_4 \bar{p}_3 \bar{p}_2 \bar{p}_1 \\
\beta'_6 &= p_1 p_2 p_3 p_4 p_5 q_6 \bar{p}_5 \bar{p}_4 \bar{p}_3 \bar{p}_2 \bar{p}_1
\end{aligned} \tag{9}$$

After appropriate grouping of terms one finds that the secondary path coefficients can be expressed in terms of the primary path coefficients (9) as follows

$$\begin{aligned}
\beta''_1 &= 0 \\
\beta''_2 &= 0 \\
\beta''_3 &= \beta'_2 q_2 \bar{q}_1 \\
\beta''_4 &= \beta'_3(\bar{q}_2 q_3 + \bar{q}_1 q_2) + \beta'_2(\bar{q}_1 q_3 \bar{p}_2 p_2) \\
\beta''_5 &= \beta'_4(\bar{q}_3 q_4 + \bar{q}_2 q_3 + \bar{q}_1 q_2) + \beta'_3(\bar{q}_2 q_4 \bar{p}_3 p_3 + \bar{q}_1 q_3 \bar{p}_2 p_2) + \beta'_2(\bar{q}_1 q_4 \bar{p}_2 p_2 \bar{p}_3 p_3) \\
\beta''_6 &= \beta'_5(\bar{q}_4 q_5 + \bar{q}_3 q_4 + \bar{q}_2 q_3 + \bar{q}_1 q_2) + \beta'_4(\bar{q}_3 q_5 \bar{p}_4 p_4 + \bar{q}_2 q_4 \bar{p}_3 p_3 + \bar{q}_1 q_3 \bar{p}_2 p_2) \\
&\quad + \beta'_3(\bar{q}_2 q_5 \bar{p}_3 p_3 \bar{p}_4 p_4 + \bar{q}_1 q_4 \bar{p}_2 p_2 \bar{p}_3 p_3) + \beta'_2(\bar{q}_1 q_5 \bar{p}_2 p_2 \bar{p}_3 p_3 \bar{p}_4 p_4)
\end{aligned} \tag{10}$$

The expressions in (9) and (10) can be generalized for a transition region divided into k sections. Thus, considering only primary and secondary path contributions in (6), one has

$$\begin{aligned}
\beta_1 &= \beta'_1 = q_1 \\
\beta_2 &= \beta'_2 = p_1 q_2 \bar{p}_1 \\
\beta_m &= q_m \prod_{j=1}^{m-1} p_j \bar{p}_j + \sum_{n=1}^{m-2} \left[\beta'_{m-n} \sum_{i=1}^{m-n-1} \left(\bar{q}_i q_{i+n} \prod_{j=1}^{n-1} \bar{p}_{i+j} p_{i+j} \right) \right], \qquad m = 3, 4, \ldots, k+1.
\end{aligned} \tag{11}$$

The first and second terms on the right hand side of the expression for β_m are the respective general forms for the primary (9) and secondary (10) path contributions.

It will be useful to consider secondary path contributions in the second time zone for reference in a later example. The expressions for β''_m in the second time zone of Fig. 1(b) are

$$\begin{aligned}
\beta''_7 &= s_1 \beta'_6 + s_2 \beta'_5 + s_3 \beta'_4 + s_4 \beta'_3 + s_5 \beta'_2 \\
\beta''_8 &= s_2 \beta'_6 + s_3 \beta'_5 + s_4 \beta'_4 + s_5 \beta'_3 \\
\beta''_9 &= s_3 \beta'_6 + s_4 \beta'_5 + s_5 \beta'_4 \\
\beta''_{10} &= s_4 \beta'_6 + s_5 \beta'_5 \\
\beta''_{11} &= s_5 \beta'_6
\end{aligned} \tag{12a}$$

where

$$\begin{aligned}
s_1 &= \bar{q}_1 q_2 + \bar{q}_2 q_3 + \bar{q}_3 q_4 + \bar{q}_4 q_5 + \bar{q}_5 q_6 \\
s_2 &= \bar{q}_1 q_3 \bar{p}_2 p_2 + \bar{q}_2 q_4 \bar{p}_3 p_3 + \bar{q}_3 q_5 \bar{p}_4 p_4 + \bar{q}_4 q_6 \bar{p}_5 p_5 \\
s_3 &= \bar{q}_1 q_4 \prod_{i=2}^{3} \bar{p}_i p_i + \bar{q}_2 q_5 \prod_{i=3}^{4} \bar{p}_i p_i + \bar{q}_3 q_6 \prod_{i=4}^{5} \bar{p}_i p_i \\
s_4 &= \bar{q}_1 q_5 \prod_{i=2}^{4} \bar{p}_i p_i + \bar{q}_2 q_6 \prod_{i=3}^{5} \bar{p}_i p_i \\
s_5 &= \bar{q}_1 q_6 \prod_{i=2}^{5} \bar{p}_i p_i
\end{aligned} \tag{12b}$$

If third and higher order contributions are ignored in the second time zone, $\beta_m = \beta''_m$. Generalizing (12a) and (12b) one has

$$\beta_m = \sum_{n=m-(k+1)}^{k} s_n \beta'_{m-n}, \qquad m = k+2, k+3, \ldots, 2k+1 \tag{13a}$$

where

$$\begin{aligned} s_1 &= \sum_{j=1}^{k} \bar{q}_j q_{j+1} \\ s_n &= \sum_{j=1}^{k+1-n} \bar{q}_j q_{j+n} \prod_{i=j+1}^{j+n-1} \bar{p}_i p_i, \qquad n = 2, 3, \ldots, k \end{aligned} \tag{13b}$$

Expressions for the transmission path coefficients in the first time zone can also be deduced by examining the path network of Fig. 1(b) and can be written as

$$\begin{aligned} \alpha_1 &= \prod_{i=1}^{k+1} p_i \\ \alpha_2 &= \alpha'_2 = \alpha_1 \sum_{i=2}^{k+1} (q_i \bar{q}_{i-1}) \\ \alpha_m &= \alpha_1 \sum_{i=m}^{k+1} \left(q_i \bar{q}_{i-m+1} \prod_{j=1}^{m-2} p_{i-j} \bar{p}_{i-j} \right) + \frac{1}{2\alpha_1} \sum_{i=2}^{m-1} \alpha'_i \alpha'_{m-i+1} \qquad m = 3, 4, \ldots, k+1. \end{aligned} \tag{14}$$

The first term on the right hand side of the expression for α_m gives the primary path contribution and the second term is an approximate representation for the secondary path contribution. It is generally sufficient to include the latter in an approximate way since secondary path contributions are significant only at the tail of the transmitted pulse.

3. RESULTS FOR ELASTIC BARS

Notation defining the geometry of the specimens is shown in Fig. 1(a). The diameter of the small end of the bar is D_1, that of the large end is D_2, and the corresponding cross sectional areas are A_1 and A_2 respectively. The coordinate measured along the cone axis is x and the origin is at the projected cone apex. Truncation planes for the transition are at positions x_1 and x_2.

The particular geometry of the transition region is immaterial in the analysis and enters the computations only through (3) and (4). If however the transition shape is a cone, the results of a given calculation set for α_m and β_m depend only on x_1 and x_2 once the number of elements k is chosen. Thus, changes in the terminating diameters affect only the apical angle and this is immaterial in the problem, unless the angle is large enough to invalidate the assumptions underlying the analysis. The coordinates x_1 and x_2 can be expressed in any units since the input pulse duration is automatically scaled through the definition of Δt. The geometry of the bars used in the experiments is given in Table 1.

In the previous section it was indicated that for moderate values of the overall area ratio, A_2/A_1, calculations for β_m and α_m could be restricted to primary and secondary paths in the first time zone without significant error. Thus for bars 1–5 β_m and α_m were given by (11) and (14) respectively. The geometry of bar 6 was extreme, however, in the sense that

TABLE 1. GEOMETRY OF EXPERIMENTAL SPECIMENS

	Bar dimensions in inches								
Bar	x_1	x_2	D_1	D_2	d_1	d_2	L_1	L_2	Material
1	$\frac{1}{2}$	1	$\frac{1}{2}$	1	$7\frac{1}{2}$	$7\frac{1}{2}$	15	20	Commercial†
2	2	4	$\frac{1}{2}$	1	7	7	16	22	Aluminum
3	4	8	$\frac{1}{2}$	1	10	10	20	20	(6061-T651)
4	8	10	$\frac{1}{2}$	$\frac{5}{8}$	7	7	16	22	
5	8	16	$\frac{1}{2}$	1	9	9	18	24	
6	1	8	$\frac{1}{8}$	1		$4\frac{1}{2}$	8	9	
7	4	8	$\frac{1}{2}$	1	10	10	20	20	Polymethyl-methyacrylate

† Wave speed $c = 20{\cdot}0 \times 10^4$ in/sec.

the overall area ratio was $A_2/A_1 = 64$. In considering the reflected pulse for this bar it was necessary to extend the calculations to the second time zone using (13a), (13b).

A set of calculated coefficients in the first time zone for bar 3 is shown graphically in Fig. 2. The stepped curves are the net pulses of transmission and reflection arising from a rectangular incident pulse of unit amplitude. Results for propagation in the positive and negative x directions are designated $T_u(4, 8)$, $R_u(4, 8)$ and $T_u(8, 4)$ $R_u(8, 4)$ respectively. In this notation the figures in parentheses are the terminating coordinates of the transition and the order in which they appear depends on the propagation direction of the incident

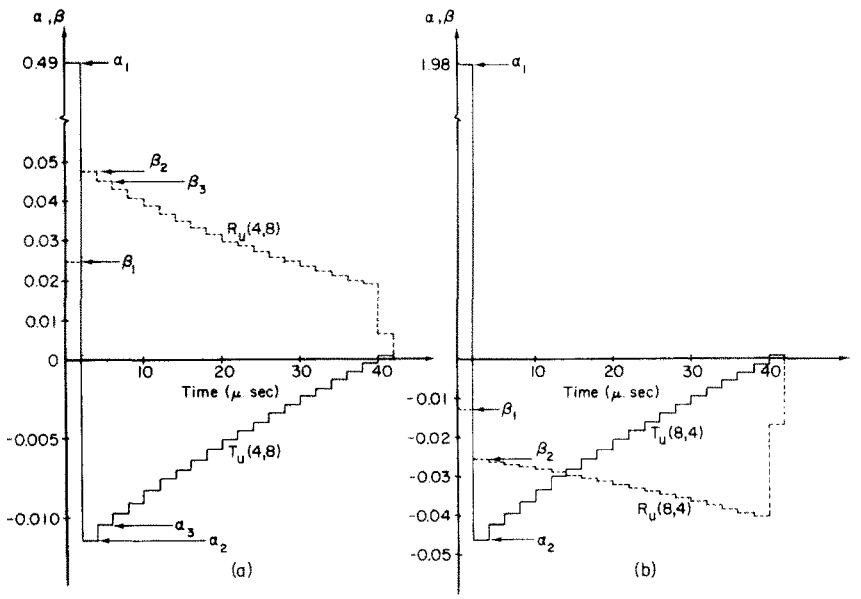

FIG. 2. Reflection and transmission curves due to unit rectangular incident pulse. (a) Small end to large end. (b) Large end to small end.

pulse. Thus, for example, $R(x_1, x_2)$ and $R(x_2, x_1)$ are the reflections due to an arbitrary incident pulse propagating in the positive and negative x directions respectively. The subscript u indicates that the curves correspond to a unit rectangular incident pulse. In the figure the reflection and transmission curves are drawn on the same time scale for convenience, but the transmitted pulse is actually delayed by an amount L/c relative to the reflective pulse.

The transition region of bar 3 was divided into 20 elements and there are thus 21 transmission and reflection coefficients in the first time zone. The first and last steps of the reflection curves [Figs. 2(a) and (b)] are about half the height of the respective adjacent steps. This results from the fact that the jumps in diameter associated with the first and last impedance elements [Fig. 1(a)] are approximately half that of the adjacent elements. The basic time increment in Fig. 2 is $\Delta t = 2{\cdot}0\,\mu$ sec so that the durations of the transmitted and reflected portions of the pulse are $42\,\mu$ sec. In fact the pulses are infinitely long but the contributions along trajectories in time zone 2 and beyond can be neglected and are not shown. For clarity, the vertical scales in Fig. 2 are exaggerated below the time axes.

The procedure for calculating the transmitted and reflected portion of an arbitrary input pulse requires superposition of the results for each discrete rectangular input. Thus if an arbitrary input pulse $I(t)$ has a time duration τ, it can be decomposed into $Q = \tau/\Delta t$ rectangular pulses where $\Delta t = 2\Delta x/c$. If the incident pulse impinges on the transition at $t = 0$, the reflection $R(t)$ and transmission $T(t)$ are given respectively by

$$R(t) = \sum_{n=1}^{Q} I(n\Delta t)\,.\,R_u(t - n\Delta t) \tag{15}$$

$$T(t) = \sum_{n=1}^{Q} I(n\Delta t)\,.\,T_u(t - n\Delta t - L/c). \tag{16}$$

The functions R_u and T_u are determined for each bar specimen, as in Fig. 2. These functions will depend upon the choice of k. Thus if k is doubled there will be twice as many steps (Fig. 2) each of which is halved in width. Noting that $|q| \sim 1/k$ it is clear that at a given value of the time, the step height will be approximately halved if k is doubled. However, apart from improved accuracy as k increases, the results given by (15) and (16) are substantially independent of k since $Q \sim k$. The choice of k is therefore chiefly a matter of convenience.

Experimental pulses were produced by the impact of a small steel sphere on an end of the specimen. The sphere was soldered to a fine steel wire and suspended from a pivot in the configuration of a pendulum. With this arrangement the impact speed was readily controlled and the pulses were therefore reproducible in a bar of given diameter. Contact between sphere and specimen served to trigger the oscilloscope sweep via a time delay circuit. The delay was set equal to the travel time of the pulse from the impact end of the specimen to the first pair of strain gauges. The gauge pairs shown in Fig. 1 ($G_1 - G_2$, $G_3 - G_4$) were connected in series to nullify the effects of any bending waves present and the output of each pair was displayed on one trace of the oscilloscope.

Some typical experimental results are shown in Figs. 3(a–d). In Fig. 3(a), the first pulse on the lower trace is the input pulse travelling in the positive x direction detected at the first gauge station on bar number 5. The second pulse on the lower trace is the reflection $R(8, 16)$ detected at the first gauge station. The pulse on the upper trace is the transmission $T(8, 16)$ detected at the second gauge station.

In Fig. 3(b) corresponding results are shown for bar number 1. The reflected pulse $R(\frac{1}{2}, 1)$ and the transmitted pulse $T(\frac{1}{2}, 1)$ are shown on the lower and upper traces respectively. Although the incident pulses are identical in Figs. 3(a) and 3(b), a marked difference is found in the shapes and durations of the reflections. On the other hand the transmitted pulses have about the same shape but differ in amplitude and duration. The specimens used for the experiments in Figs. 3(a, b) (bars 5 and 1 respectively) are identical except for the length of the transition region.

The upper trace in Fig. 3(c) shows an incident pulse propagating in the negative x direction followed by the reflected pulse in bar 5. The transmitted pulse appears on the lower trace. Oscillations in the tail of the transmitted pulses result from the effects of lateral inertia which are not completely absent in the experiments. This occurs because of the presence of high frequency components in the Fourier spectrum of the incident pulse.

Figure 3(d) shows the displacement profile of the transmitted pulse in bar number 6. The pulse input was in the negative x direction and strain gauges could not be conveniently used on the small end of the bar. The pulse was therefore detected using a condenser microphone, of the type devised by Davies [8], at the free end on the transmission side of the specimen.

The relation between the geometrical properties of the bars and the character of the transmitted and reflected pulses is illustrated by grouping the results in three categories: (a) the transition length, L, is fixed and x_1 is varied; (b) x_1 is fixed and L is varied; (c) x_1 and L are varied but the area ratio A_2/A_1 is fixed. Thus one can imagine constructing the specimens by removing various sections from a cone of given apical angle and inserting them between cylindrical end sections of appropriate diameters. In practice, however, it is convenient to use a sequence of bars with the same end diameters and adjust the cone angle to achieve the variations in (a), (b) and (c) above. As indicated earlier, the cone angle is not a parameter in the problem.

Since most of the bars had end diameters of $\frac{1}{2}$ in. and 1 in. it was possible to use two standard incident pulses for the calculations. In the particular case of bar number 4, for which one end had a diameter of $\frac{5}{8}$ in., the input pulse shape was nearly identical to that observed for 1 in. diameter bars. To facilitate comparisons, the incident pulse amplitude for bar number 4 was normalized to match that for 1 in. diameter bars. The experimental transmitted and reflected pulses for this bar were scaled by the same factor. In the case of bar 6 there were no experiments involving impact on the small end of the bar.

In Figs. 4 and 5 calculated and experimental results are shown for bars 2 and 4 and for an "imaginary" bar (dashed line) in which the transition length is constant at 2 in. As the transition region is taken nearer the cone apex in Fig. 4 the transmission amplitude decreases and the reflection amplitude increases. The reverse is observed in Fig. 5. In addition the reflected and incident pulses are of like sign in Fig. 4 and of opposite sign in Fig. 5. The experimental and calculated pulses for bars 2 and 4 are evidently in satisfactory agreement.

In these and subsequent figures the pulse amplitudes are given in units of stress with compression positive. The amplitude is irrelevant as long as the elastic range of the material is not exceeded, but is shown for reference.

The results illustrated in Fig. 6 show that as L increases for fixed x_1, there is a sharp decrease in transmission amplitude without a significant change in shape. However, the duration of the reflected pulse increases markedly as L increases while the peak amplitude remains nearly constant.

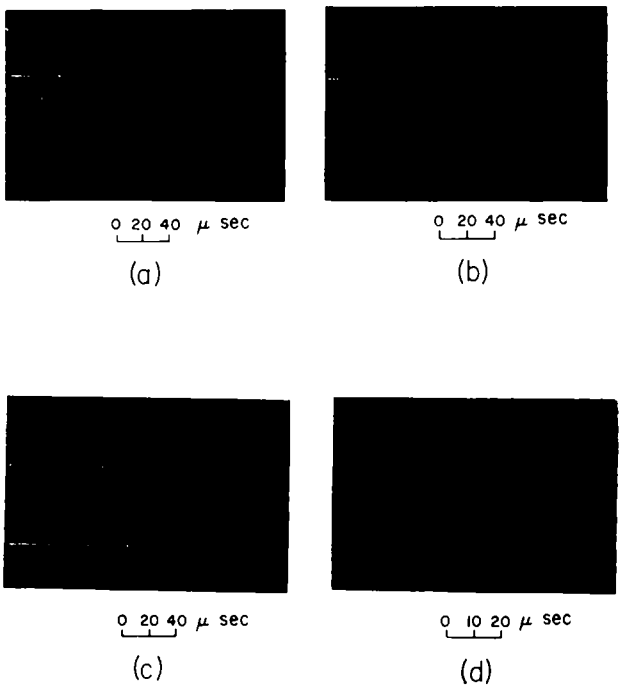

FIG. 3. Experimental pulses. (a) Bar 5. (b) Bar 1. (c) Bar 5. (d) Bar 6. (a)—(c) Stress profiles. (d) Displacement profile (positive downward).

facing p. 528

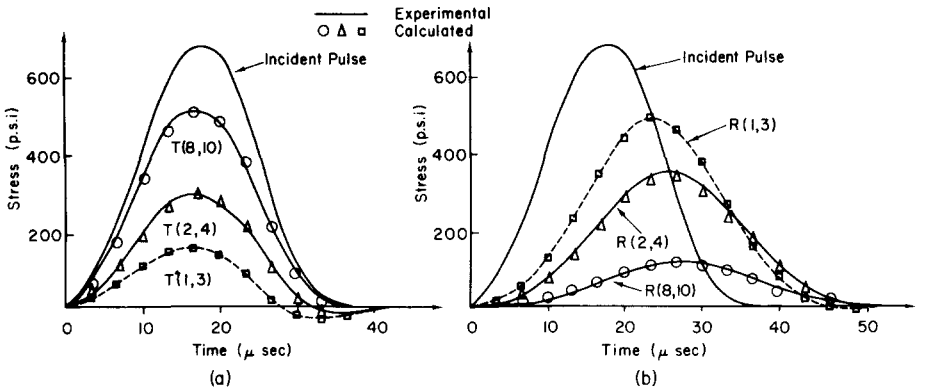

FIG. 4. Calculated and experimental pulses for fixed transition length (small end to large end). (a) Transmission. (b) Reflection.

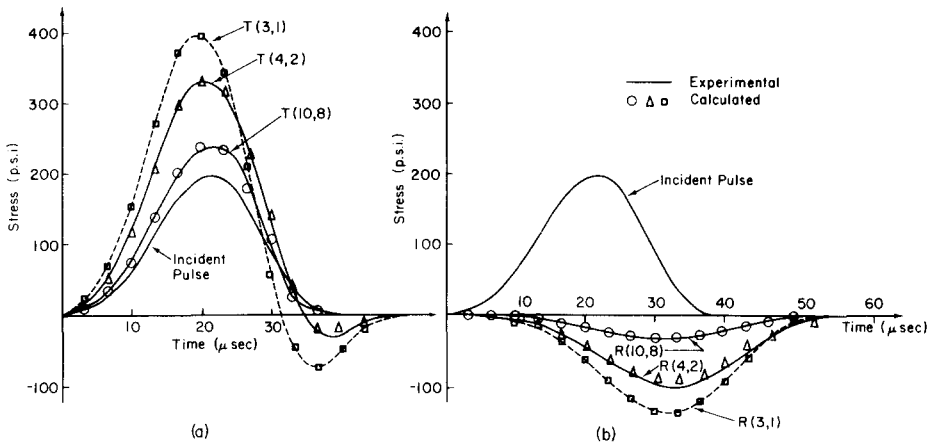

FIG. 5. Calculated and experimental pulses for fixed transition length (large end to small end). (a) Transmission. (b) Reflection.

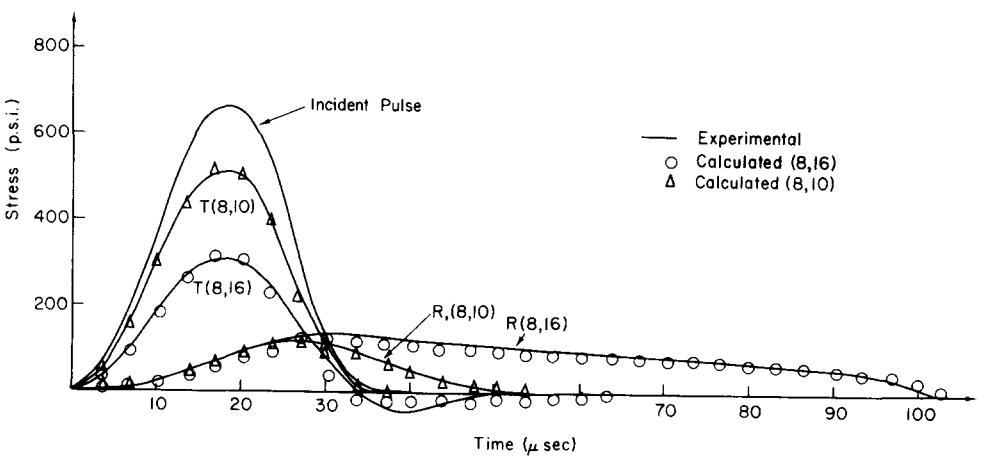

FIG. 6. Transmitted and reflected pulses for fixed x_1 (small end to large end).

In Fig. 7 results are shown for three bars in which the area ratio is fixed, i.e. $A_2/A_1 = 4$, as L and x_1 are varied. The three transmission pulses were nearly identical and one of them, $T(16, 8)$, is deleted from the figure for clarity. These results together with those of Figs. 4, 5 and 6 indicate that the transmission shape is not strongly affected by changes in the transition parameters. When the area ratio varies, the effect on the transmission is chiefly in amplitude. An exception occurs in extreme situations where $A_2/A_1 \gg 1$, in which case a significant tail develops in the transmitted pulse. Such an example is discussed in connection with Fig. 8.

The reflected pulses in Fig. 7 are significantly different in amplitude and duration even though A_2/A_1 is fixed. From the previous results it is clear that for a given incident pulse the reflection amplitude depends on the proximity of the transition to the cone apex and the duration depends on the transition length.

In the case of bar 1 in Fig. 7 the ratio of spatial pulse length to transition length is about 16. The transmission and reflection pulse shapes, $T(1, \frac{1}{2})$ and $R(1, \frac{1}{2})$ are nearly identical to the incident pulse and their amplitudes are about the same experimentally as would be given by treating the transition as a single abrupt step. Thus the ratios of peak experimental amplitudes in the figure are $\sigma_r/\sigma_i \simeq -0{\cdot}6$, $\sigma_t/\sigma_i \simeq 1{\cdot}6$ and the same results are obtained from (1) and (2) taking $A_2/A_1 = 4$. Similar results are found when the incident pulse propagates from the small end to the large end [Fig. 3(b)]. Hence, if the dominant wavelengths of a pulse are large compared to L, the details of the transition region can be ignored and it can be treated as an abrupt change.

In Fig. 8 the reflected and transmitted pulse shapes are shown for an incident pulse propagating from the large end to the small end in bar 6. Here, the cross sectional area is reduced by a factor of 64 and the pulse very nearly reaches the cone apex. The small end of bar 6 was only $\frac{1}{8}$ in. in diameter and detection of the transmitted pulse by means of strain gauges was thus impractical. The free end displacement was observed instead using a

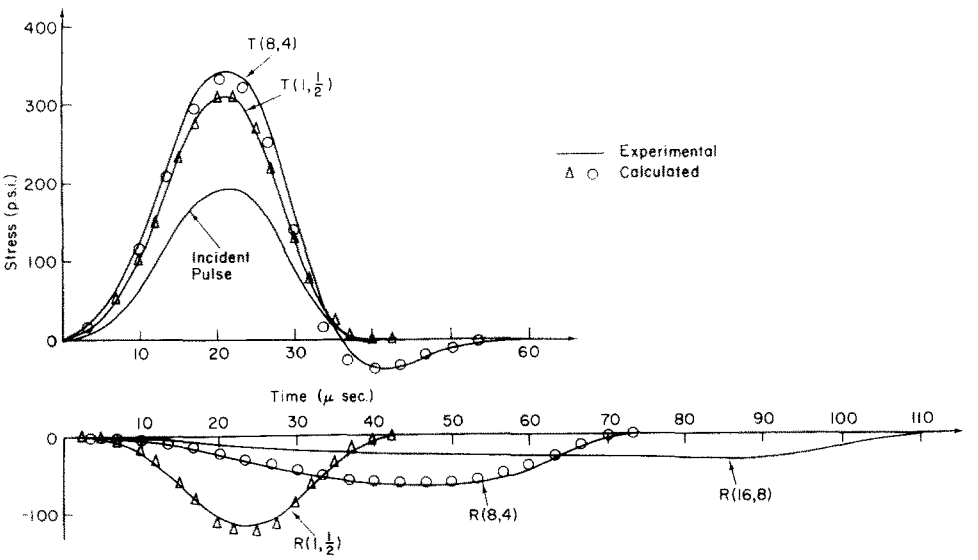

FIG. 7. Transmitted and reflected pulses for fixed overall area ratio.

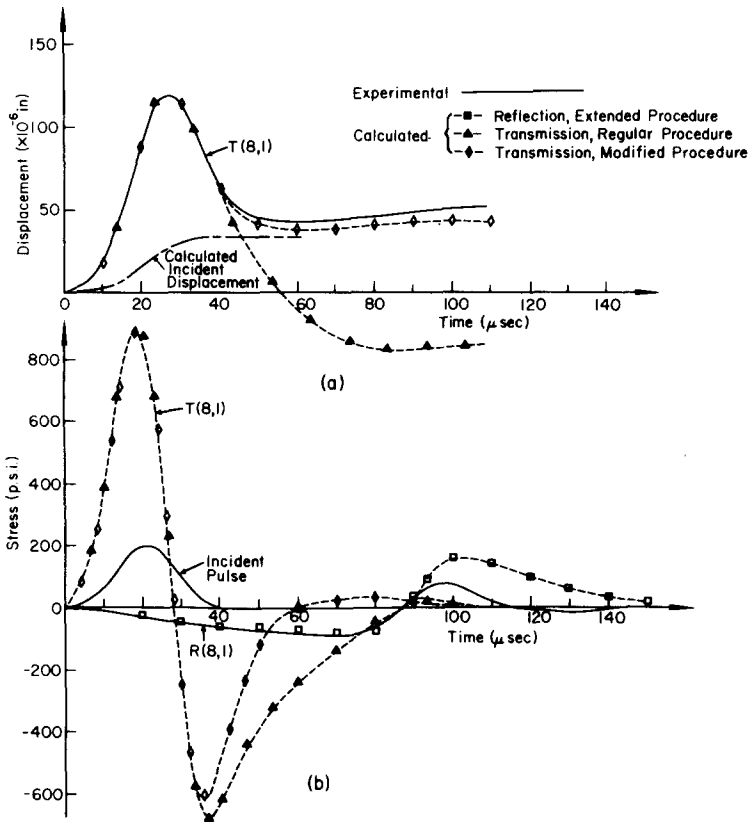

FIG. 8. Transmitted and reflected pulses in bar 6 (large end to small end). (a) Transmitted displacement profile. (b) Stress profiles.

condenser microphone [8]. Displacement profiles were also calculated from corresponding stress profiles by numerical integration of the latter according to the well known relation between stress and the time derivative of displacement at the free end of an elastic bar, i.e. $\sigma = (\rho c \partial u/\partial t)/2$, [7].

The stress profile of the transmitted pulse was calculated using both the "regular procedure", based on (14) and (16), and a "modified procedure". In the modified procedure the transition was first divided into 3 subregions, each having a moderate overall area ratio $A_2/A_1 = 4$. The transmission through each subregion was calculated using the regular procedure. Each transmission was then used as the input to the next subregion together with back reflections from the previous one. This was continued until the final transmitted pulse was obtained. By using the modified procedure it is possible to circumvent the direct need for higher order paths and several time zones in calculations for bars with large overall area ratios.

In comparing the calculated and experimental displacement profiles [Fig. 8(a)] it is clear that the regular procedure gives satisfactory results only over the head of the pulse. In the tail region, however (beyond 40 μ sec), the results of the regular procedure are in

poor agreement with experiment. The discrepancy arises for two reasons: (a) in the time between 40 μ sec and the end of the first time zone (70 μ sec) the error is primarily due to the approximate way in which secondary path contributions are included in (14). This approximate expression underestimates the contribution of secondary paths; (b) the regular procedure totally omits the secondary (and higher order) path contributions in the domain beyond the first time zone. The results of the modified procedure are however in satisfactory agreement with experiment.

For the reflected pulse, the exact contributions of primary and secondary paths are included in the first time zone. In the second time zone the exact contributions of secondary paths are included using (11) and (13a, b) and this is termed the "extended procedure". Comparison between calculated and experimental reflection pulses [Fig. 8(b)] indicates satisfactory agreement over the main portion (up to 90 μ sec) and less satisfactory agreement thereafter. The discrepancy between calculation and experiment in the tail of the reflected pulse results from the omission of third order path contributions in the second time zone.

When the incident pulse propagates in the negative x direction the signs of odd order path contributions are negative. As the positive contributions of secondary paths diminish in the second time zone, the third order contributions become dominant. This accounts for the oscillations in the tail of the reflected pulse in Fig. 8(b). These oscillations persist indefinitely as successive path orders dominate, but with decreasing amplitude. Similar oscillations are present in the reflected pulses in other bars, but their amplitudes are smaller relative to the main part of the pulse.

For each of the bars used in the experiments, and a number of fictitious bars, calculations were carried out to determine the momentum associated with the transmitted and reflected portions of a rectangular incident pulse. This was done by numerically integrating over the time duration of the stress pulse and multiplying by the cross sectional area of the bar. The ratio of the momenta associated with reflection and transmission (M_R/M_I, M_T/M_I respectively) is plotted against area ratio in Fig. 9. The momentum ratios depend only on

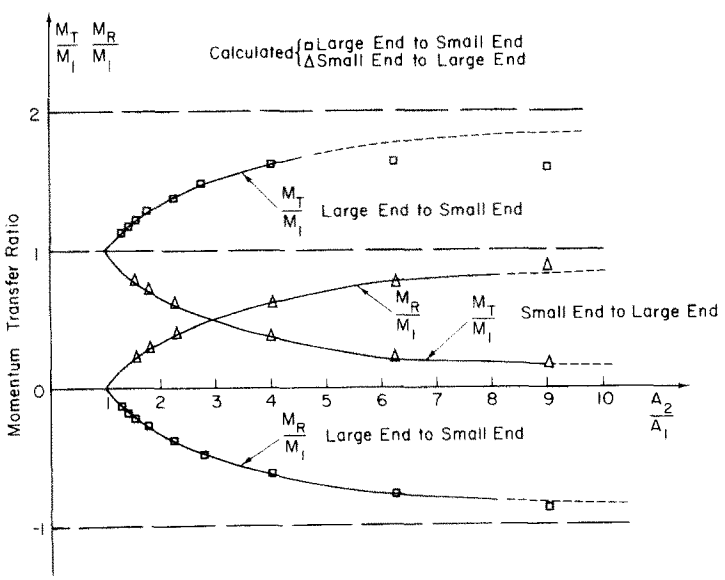

FIG. 9. Momentum ratio vs. overall area ratio.

A_2/A_1 as is illustrated by the reflection pulses in Fig. 7 which vary in shape and amplitude but enclose equal areas.

4. NONUNIFORM VISCOELASTIC BARS

Kolsky and Lee considered pulse propagation along a composite bar formed by joining two dissimilar viscoelastic bars of the same cross section and deduced the counterparts of (1) and (2). The simpler result needed for the present case, in which only the area is changing, may be obtained by beginning with the complex modulus representation for a linear viscoelastic solid under uniaxial stress [9]

$$\sigma = (E_1 + iE_2)\frac{\partial u}{\partial x} \tag{17}$$

where $\partial u/\partial x$ is the strain and E_1 and E_2 are the real and imaginary parts of the complex modulus respectively. Let a sinusoidal wave of angular frequency p propagate in the positive x direction and encounter an area jump A_j to A_{j+1} at $x = 0$. The incident, reflected, and transmitted displacement profiles will have different amplitudes and can be represented in the respective forms [2, 9]

$$\begin{aligned} u_i &= \overline{U}\exp[-\gamma x + ip(t - x/c)] \\ u_r &= \overline{V}\exp[\gamma x + ip(t + x/c)] \\ u_t &= \overline{W}\exp[-\gamma x + ip(t - x/c)] \end{aligned} \tag{18}$$

where γ and c are the frequency dependent attenuation and phase velocity respectively, and $\overline{U} = U_1 + iU_2$, $\overline{V} = V_1 + iV_2$, $\overline{W} = W_1 + iW_2$ are the complex amplitudes. Convenient expressions for γ and c are available from the linear theory of viscoelasticity. Thus, one has [9]

$$\gamma = \frac{p\tan\delta/2}{c} \tag{19}$$

where δ is the phase angle between stress and strain and is defined by $\tan\delta = E_2/E_1$. For many linear viscoelastic solids $\tan\delta$ is approximately constant (independent of frequency) and is small compared to unity. When these conditions hold it is possible to show that [10, 11]

$$c = c_0\left[1 + \frac{\tan\delta}{\pi}\ln(p/p_0)\right] \tag{20}$$

where p_0 is a reference frequency and c_0 is the speed at that frequency.

The viscoelastic bar used in the present experiments (bar 7) was made of polymethylmethacrylate. In this material $\tan\delta \simeq 0{\cdot}036$ over the range of frequencies in the Fourier spectrum of the experimental pulse [12].

It is required that the displacement be continuous at $x = 0$, i.e.

$$\overline{U} + \overline{V} = \overline{W} \tag{21}$$

and that the forces balance at the jump

$$[(\sigma_i + \sigma_r)A_j = \sigma_t A_{j+1}]_{x=0}. \tag{22}$$

Using (17), (18), (21) and (22) one finds

$$\begin{aligned} W_1 &= p_j U_1, \qquad W_2 = p_j U_2 \\ V_1 &= -q_j U_1, \qquad V_2 = -q_j U_2. \end{aligned} \tag{23}$$

Substituting each displacement of (18) into (17), taking the real or imaginary part, and using (23), one finds that the incident, reflected, and transmitted stress amplitudes at $x = 0$ are related as in (1) and (2). Similarly the relations between the strains at $x = 0$ are $\varepsilon_r = q_j \varepsilon_i$, $\varepsilon_t = p_j \varepsilon_i$ (or $\varepsilon_r = \bar{q}_j \varepsilon_i$, $\varepsilon_t = \bar{p}_j \varepsilon_i$). In the viscoelastic case it is appropriate to deal with the strains since it is the strains which are measured. The stress and strain profiles of a viscoelastic pulse are not identical as in the case of elastic solids [2].

Thus the calculations for α_m and β_m in a homogeneous, nonuniform viscoelastic bar depend only on geometry just as in the elastic case. The viscoelastic specimen used in the experiments (bar 7) had the same geometry as one of the elastic bars (bar 3) and the previously calculated coefficients could therefore be used again. However, in the viscoelastic case one must account for the effects of dispersion and attenuation as a pulse propagates along each uniform element of the transition. This necessitates a harmonic analysis.

Consider now an arbitrary pulse propagating toward the transition region along one of the uniform end sections of a viscoelastic bar. If the strain pulse is observed at one of the gauge stations it can be represented by a truncated Fourier series in the form

$$\varepsilon_i = \sum_{n=0}^{N} A_n \exp(inp_0 t)$$

where p_0 is an appropriate reference frequency, and A_n is a complex constant given by $A_n = a_n - ib_n$. The upper limit of the summation, N, is chosen large enough to obtain an accurate representation of the pulse. The coefficients a_n, b_n can be determined numerically for an arbitrary pulse using the usual Fourier methods and are therefore regarded as known.

Let x' be a coordinate axis which is positive in the propagation direction of the incident pulse and which has its origin at the start of the transition region. Thus referring to Fig. 1(a), if the incident pulse propagates from the small end to the large end one has $x' = x - x_1$, and if the pulse propagates in the opposite direction $x' = x_2 - x$. Consider for example the former case in which the pulse propagates a distance d_1 between the first gauge station and the transition. Then at $x' = 0$ one has

$$\varepsilon_i(0, t) = \sum_{n=0}^{N} A_n \exp[-\gamma_n d_1 + inp_0(t - d_1/c_n)] \tag{24}$$

where γ_n and c_n are the damping coefficient and phase velocity respectively for the nth harmonic [(19) and (20)]. It is convenient to make the substitution $t_1 = t - d_1/v$, where v is the approximate pulse speed, so that the time coordinate system moves with the pulse. Thus, taking the real part of (24), expanding and collecting terms, one has

$$\varepsilon_i(0, t_1) = \sum_{n=1}^{N} (a_n^* \cos np_0 t_1 + b_n^* \sin np_0 t_1) + a_0 \tag{25a}$$

where

$$a_n^* = \exp(-\gamma_n d_1)\left[a_n \cos np_0\left(\frac{d_1}{v} - \frac{d_1}{c_n}\right) + b_n \sin np_0\left(\frac{d_1}{v} - \frac{d_1}{c_n}\right)\right]$$

$$b_n^* = \exp(-\gamma_n d_1)\left[b_n \cos np_0\left(\frac{d_1}{v} - \frac{d_1}{c_n}\right) - a_n \sin np_0\left(\frac{d_1}{v} - \frac{d_1}{c_n}\right)\right]. \tag{25b}$$

The reflected and transmitted waves are composed of contributions along the respective exit trajectories of Fig. 1(b) and the amplitude of each contribution is obtained using the appropriate reflection or transmission coefficient. The reflection and transmission coefficients are attenuated in the viscoelastic case according to the total path length associated with each trajectory. The path length for the reflection trajectories can be written in the form $\Delta s_m = (m-1)2\Delta x$ and for the transmission trajectories the path lengths are $\Delta s_m + L$. For a given frequency the times between exit trajectories are equal and are given by $\Delta t_n = 2\Delta x/c_n$. Thus, assuming the reflection and transmission pulses are adequately represented by contributions in the first time zone, one has at $x' = 0$ and $x' = L$ respectively:

$$\varepsilon_r(0, t_1) = \sum_{n=1}^{N}\sum_{m=1}^{k+1} \beta_m \exp(-\gamma_n \Delta s_m)\{a_n^* \cos np_0[t_1 - (m-1)\Delta t_n] + b_n^* \sin np_0[t_1 - (m-1)\Delta t_n]\} + a_0 \sum_{m=1}^{k+1} \beta_m \tag{26}$$

$$\varepsilon_t(L, t_2) = \sum_{n=1}^{N}\sum_{m=1}^{k+1} \alpha_m \exp[-\gamma_n(\Delta s_m + L)]\left\{a_n^* \cos np_0\left[t_2 + \frac{L}{v} - \frac{L}{c_n} - (m-1)\Delta t_n\right] + b_n^* \sin np_0\left[t_2 + \frac{L}{v} - \frac{L}{c_n} - (m-1)\Delta t_n\right]\right\} + a_0 \sum_{m=1}^{k+1} \alpha_m \tag{27}$$

where $t_2 = t_1 - L/v$.

Equations (26) and (27) can be rewritten in the respective forms:

$$\varepsilon_r(0, t_1) = \sum_{n=1}^{N} [a_n^r \cos np_0 t_1 + b_n^r \sin np_0 t_1] + a_0 \sum_{m=1}^{k+1} \beta_m \tag{28}$$

$$\varepsilon_t(L, t_2) = \sum_{n=1}^{N} [a_n^t \cos np_0 t_2 + b_n^t \sin np_0 t_2] + a_0 \sum_{m=1}^{k+1} \alpha_m \tag{29}$$

where

$$a_n^r = \sum_{m=1}^{k+1} \{\exp(-\gamma_n \Delta s_m)\beta_m[a_n^* \cos np_0(m-1)\Delta t_n - b_n^* \sin np_0(m-1)\Delta t_n]\}$$

$$b_n^r = \sum_{m=1}^{k+1} \{\exp(-\gamma_n \Delta s_m)\beta_m[b_n^* \cos np_0(m-1)\Delta t_n + a_n^* \sin np_0(m-1)\Delta t_n]\} \tag{30a}$$

$$a_n^t = \sum_{m=1}^{k+1} \left\{ \exp[-\gamma_n(\Delta s_m + L)]\alpha_m \left(a_n^* \cos np_0 \left[\frac{L}{c_n} - \frac{L}{v} + (m-1)\Delta t_n \right] \right. \right.$$
$$\left. \left. - b_n^* \sin np_0 \left[\frac{L}{c_n} - \frac{L}{v} + (m-1)\Delta t_n \right] \right) \right\}$$
$$b_n^t = \sum_{m=1}^{k+1} \left\{ \exp[-\gamma_n(\Delta s_m + L)]\alpha_m \left(b_n^* \cos np_0 \left[\frac{L}{c_n} - \frac{L}{v} + (m-1)\Delta t_n \right] \right. \right. \tag{30b}$$
$$\left. \left. + a_n^* \sin np_0 \left[\frac{L}{c_n} - \frac{L}{v} + (m-1)\Delta t_n \right] \right) \right\}$$

Thus (28) and (29) are the Fourier representations of the reflected and transmitted pulses respectively at the ends of the transition region. To facilitate comparison with experiment, each pulse must be calculated at the location of the appropriate gauge station; $x' = -d_1$ for the reflection, and $x' = d_2 + L$ for the transmission. Noting that $\gamma_0 = 0$, multiplying each term in (28) and (29) by $\exp(-\gamma_n d_1)$ and $\exp(-\gamma_n d_2)$ respectively, and making the substitution $t_1^* = t_1 - d_1/v$, and $t_2^* = t_2 - d_2/v$, one obtains

$$\varepsilon_r(-d_1, t_1^*) = \sum_{n=1}^{N} \exp(-\gamma_n d_1)\{(a_n^r \cos np_0\theta_n + b_n^r \sin np_0\theta_n)\cos np_0 t_1^*$$
$$+ (b_n^r \cos np_0\theta_n - a_n^r \sin np_0\theta_n)\sin np_0 t_1^*\} + a_0 \sum_{m=1}^{k+1} \beta_m \tag{31}$$

$$\varepsilon_t(d_2 + L, t_2^*) = \sum_{n=1}^{N} \exp(-\gamma_n d_2)\{(a_n^t \cos np_0\phi_n + b_n^t \sin np_0\phi_n)\cos np_0 t_2^*$$
$$+ (b_n^t \cos np_0\phi_n - a_n^t \sin np_0\phi_n)\sin np_0 t_2^*\} + a_0 \sum_{m=1}^{k+1} \alpha_m \tag{32}$$

where

$$\theta_n = \frac{d_1}{v} - \frac{d_1}{c_n}, \qquad \phi_n = \frac{d_2}{v} - \frac{d_2}{c_n}$$

Equations (31) and (32) are the desired final forms for the reflection and transmission strain pulses respectively. These equations account for the total distortion of a viscoelastic pulse resulting from propagation in both the uniform and transition sections.

Calculations were carried out for the reflected and transmitted pulses in a polymethylmethacrylate specimen (bar 7) based on an observed incident pulse. The basic interval of the Fourier summation was 500 μ sec which corresponds to a fundamental frequency of $p_0 = 12{\cdot}6 \times 10^3$ rad/sec. A value of $c_0 = 8{\cdot}66 \times 10^4$ in/sec was used for the wave speed appropriate to this frequency. The pulses could be adequately represented by $N = 25$ harmonics. Experimental and calculated results are shown in Fig. 10 and are evidently in satisfactory agreement. A separate calculation is shown for the same incident pulse, assuming the bar to be elastic ($\tan\delta = 0$). The elastic and viscoelastic pulses are similar but the viscoelastic effect is clearly evident.

The computations were performed with the help of a digital computer throughout.

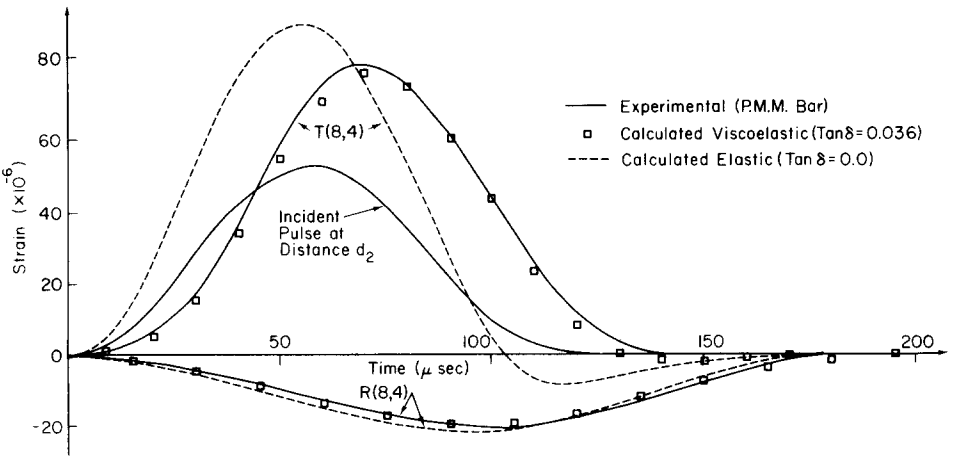

FIG. 10. Calculated and experimental pulses in bar 7 (large end to small end).

5. CONCLUDING REMARKS

A method has been presented for computing the reflected and transmitted portions of a longitudinal stress pulse propagating through a finite region of continuously variable cross section in a bar. In an elastic solid the problem is treated in terms of discrete rectangular segments of a pulse. For a viscoelastic solid in which dispersion and attenuation are significant, the elastic formulation is recast in terms of a harmonic analysis.

It has been shown that the transmitted and reflected pulse shapes are essentially the same as that of the incident pulse if the dominant wavelengths of the latter are long compared to the transition length. The amplitude of the reflection and transmission in this case can be calculated in a single step by treating the transition as an abrupt change.

The regime of greatest interest, however, is that in which the dominant pulse wavelengths are comparable to the transition length. In this regime the method presented is readily applicable for pulses and transitions of arbitrary shape.

In cases where the overall area ratio is of the order of 10 or less, the basic method of the paper works well even if computations are restricted to primary and secondary paths in the first time zone. For larger values of the area ratio the method must be modified or calculations must be carried beyond the first time zone and include third order paths and higher.

The area ratio also determines the momentum associated with the pulses of reflection and transmission. Thus, for a given area ratio, these momenta are not affected by making the transition more or less gradual. The results in Fig. 9 and the foregoing remarks apply equally in viscoelastic and elastic bars.

Finally it is clear that the method of the paper is applicable in a number of other problems. These include stress pulse propagation along uniform bars with variable mechanical properties, analogous optical problems, propagation of electromagnetic waves in a waveguide of variable cross section, and so forth. In each case it is necessary to use appropriate expressions for p_j and q_j. These coefficients may be functions of frequency in some cases but this is readily incorporated in the harmonic analysis.

REFERENCES

[1] LORD RAYLEIGH, *The Theory of Sound*, 2nd edition, Vol. 1, pp. 250–1. Macmillan (1894). (Reprinted 1945, Dover, New York).
[2] H. KOLSKY and S. S. LEE, The propagation and reflection of stress pulses in linear viscoelastic media. Brown University Technical Report No. 5, Contract Nonr 562(30), (1962).
[3] E. A. RIPPERGER and H. N. ABRAMSON, Reflection and transmission of elastic pulses in a bar at a discontinuity in cross section. *Proc. 3rd midwest. Conf. on Solid Mech.* p. 135 (1957).
[4] L. H. DONNELL, Longitudinal wave transmission and impact. *Trans. Am. Soc. Mech. Engrs* **52**, 153 (1930).
[5] R. P. REED, Stress pulse-trains from multiple reflection at a zone of many discontinuities. A notation for machine solution. Sandia Corporation Research Report 4642 (1962).
[6] U. S. LINDHOLM and K. D. DOSHI, Wave propagation in an elastic nonhomogeneous bar of finite length. *J. appl. Mech.* **87**, 135 (1965).
[7] H. KOLSKY, *Stress Waves in Solids*. Clarendon Press (1953). (Reprinted 1964, Dover, New York).
[8] R. M. DAVIES, A critical study of the Hopkinson pressure bar. *Phil. Trans. R. Soc.* **A240**, 375 (1948).
[9] H. KOLSKY, The propagation of acoustic pulses in linear viscoelastic solids. *Proc. 4th Int. Congr. on Acoustics* (1962).
[10] H. KOLSKY, The propagation of stress pulses in viscoelastic solids. *Phil. Mag.* **1**, 693 (1956).
[11] B. GROSS, *Mathematical Structure of Theories of Viscoelasticity*. Hermann (1953).
[12] W. LETHERSICH, The rheological properties of dielectric polymers. *Br. J. appl. Phys.* **1**, 294 (1950).

(*Received* 7 *May* 1969; *revised* 30 *July* 1969)

Абстракт—Исследуется распространение импульса напряжения вдоль однородных, но неравномерных стержней. Стержни имеют два равномерные концевые сечения, разных диаметров, соединенных конечной переходной зоной. Когда импульс действует на переходную зону, тогда он распространяется по бесконечной сети траекторий, ведущих до передачи и отражения. В анализе приближается переходная зона множеством скачко-образных ступеней в области. Отождествляются конечное множество траекторий, которые значительно вносят вклад в импульсы отражения и передачи. Даются расчеты для двух импульсов. Основный анализ является удобным для упругих импульсов произвольной формы. Вновь формулируется его в гармонической форме, для использования расчета вязкоупругих стержней. Находится надлежащая сходимость между численными и экспериментальными результатами.